A Lensless Retinal Scanning Display for Augmented Reality

Lantian Mi, Chao Ping Chen, Yifan Lu, Wenbo Zhang, Ming Zhu, Ruixue Tang, Xingyu Ren, and Nizamuddin Maitlo*

Smart Display Lab, Department of Electronic Engineering, Shanghai Jiao Tong University, Shanghai, China
Email: ccp@sjtu.edu.cn

Abstract

We propose a design of a retinal-scanning-based near-eye display for augmented reality. Our solution is highlighted by a scanning laser projector, a diffractive optical element, and a wet eye with gradient refractive indices. Its design rules are set forth in detail, followed by the results and discussion.

Keywords

augmented reality; near-eye display; retinal scanning; diffractive optical element; gradient refractive index.

1. Introduction

Retinal projection displays refer to a type of near-eye displays (NEDs), in which the image is directly projected to the retina. Compared to combiner-based [1-4] and waveguide-based [5-8] NEDs, this type of NEDs have an edge on achieving ultra-large field of view (FOV). However, there are also a number of issues holding them back from the applications. For example, iOptik [9] developed by Innovega, which is characterized by a contact lens with a zone plate, has been struggling for many years in persuading the consumers to wear the contact lens. Pinlight display [10], which mimics a pinhole camera by an array of point light sources in front of eye, is vulnerable to the change of eye state, including the diopter of eye, pupil size, and rotation of eyeball. Inspired from the said issues, we would like to present a lensless retinal scanning display (RSD).

2. Proposed Structure

The proposed RSD can be decomposed into three major components, *i.e.* a scanning laser projector, a diffractive optical element (DOE), and an eye, as shown in Fig. 1, where d_p is the distance between projector and glass, d_{doe} the distance between projector and DOE, d_{lens} the distance between DOE and lens center, W the horizontal dimension of DOE, x the distance starting from the left edge of DOE, θ_i the angle of incident light, and θ_m the angle of diffracted light. Inside the temple is housed the scanning laser projector to save the room. On the inner surface of a flat glass substrate is fabricated the DOE, which is able to converge the light coming out of the projector towards the center of lens of eye. Analogous to the Maxwellian view [11], such configuration ensures that the image formed on the retina will remain intact no matter how the eye accommodates its diopter to the distance of object. Moreover, as long as the beam size of the laser is way smaller than the pupil—minimally 2 mm across—the brightness of image could be maintained regardless of the variation of pupil size. For the sake of symmetry, the DOE and eye are center-aligned.

3. Design Rules

Eye: Figure 2 is a cross-sectional view of our schematic wet eye, consisting of tear, cornea (anterior and posterior), aqueous chamber filled with aqueous humor, iris with an opening known as pupil, lens (anterior and posterior), vitreous chamber filled with vitreous humor, and retina. Unlike our previous eye models [12-16], in which the eye is dry—in the absence of tear—and lens of eye has a constant refractive index, the current model factors into not only the tear but also a gradient lens. While the thickness of tear is negligibly thin—ranging from 6 to 20 μm—the irregularities of tear can cause significant visual aberrations and distortions [17].

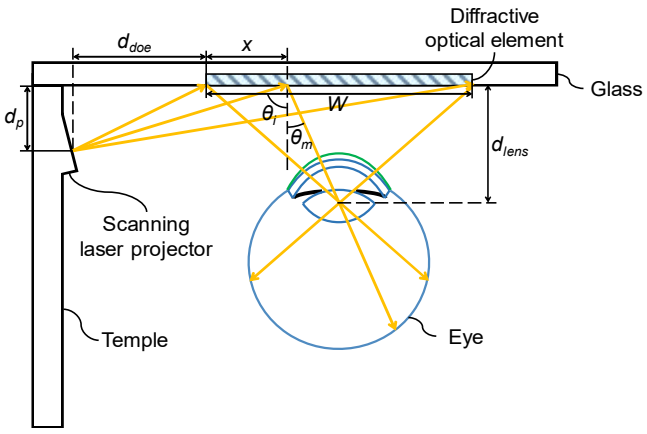

Figure 1. Schematic drawing of the proposed RSD.

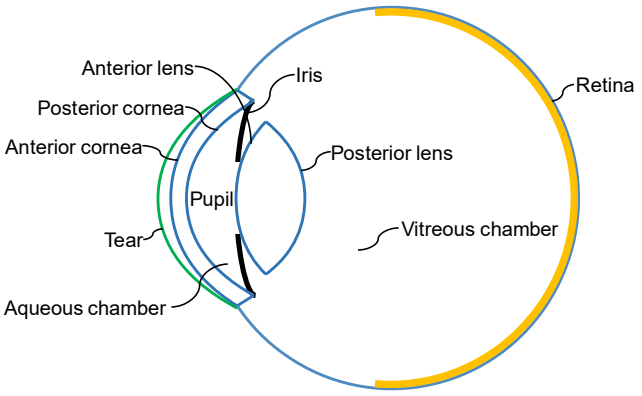

Figure 2. Cross-sectional view of our schematic wet eye.

To model the gradient lens, Goncharov's gradient lens model is adopted [18], by which refractive indices n_a for the anterior lens and n_p for the posterior lens could be computed with

$$n_a(z,y) = n_{00} + c_{10}y^2 + c_{20}y^4 + c_{01}(z+z_m) + c_{02}(z+z_m)^2 + c_{03}(z+z_m)^3 + c_{04}(z+z_m)^4 \quad (1)$$

and

$$n_p(z,y) = n_{max} + c_{10}y^2 + c_{20}y^4 + c_{01,2}z + c_{02,2}z^2 + c_{03,2}z^3 + c_{04,2}z^4 \quad (2)$$

respectively, where z is the distance measured from the vertex of anterior lens along the z-axis, y the distance measured from the lens center along the y-axis, z_m the distance between the vertex of anterior lens and the virtual plane, n_{00} the starting refractive index

of anterior lens, n_{max} the maximum refractive index, and $c10$, $c20$, c_{01}, c_{02}, c_{03}, c_{04}, $c_{01,2}$, $c_{02,2}$, $c_{03,2}$, and $c_{04,2}$ the coefficients of each term.

DOE: DOE is an array of slanted gratings, which can be fabricated with electron-beam [19], holographic [20], or nanoimprint lithography [21]. The number of slanted gratings shall match with the resolution of scanning laser projector. As shown in Fig. 3, p is the grating period, h_g the grating depth, w_g the grating width, and β the slant angle relative to the normal. All the diffracted beams are supposed to pass through the lens center. For a grating located at a distance x from the left edge of DOE, its parameters should satisfy both the reflection grating equation, *i.e.*

$$p(\sin\theta_i - \sin\theta_m) = m\lambda \tag{3}$$

and the geometry (see Fig. 1) given by

$$\tan\theta_i = \frac{d_{doe}+x}{d_p} \tag{4}$$

and

$$\tan\theta_m = \frac{W/2 - x}{d_{lens}} \tag{5}$$

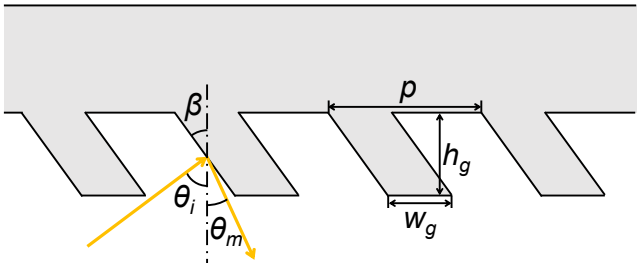

Figure 3. Cross-sectional profile of the slanted grating.

4. Results and Discussion

Simulation Settings: The performance of our RSD is quantitatively analyzed with Code V (Synopsys) and COMSOL Multiphysics (COMSOL) at the wavelength of 532 nm. Figure 4 outlines the optical surfaces used in Code V. The object is placed at 3 m ahead of the eye. Surfaces 1 to 8 (S1 to S8) constitute the wet eye, of which, S1 is tear, S2 anterior cornea, S3 posterior cornea, S4 iris with pupil, S5 anterior lens, S6 virtual plane, S7 posterior lens, and S8 retina. To imitate the scanning laser projector as a pinhole camera, the semi-aperture of virtual plane—where the lens center is located—is set as 30 μm, half the size of the laser beam.

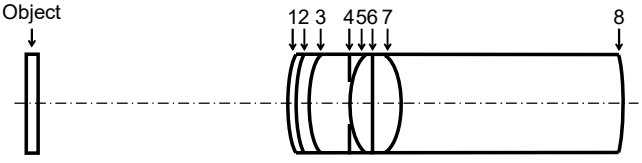

Figure 4. Numbering of surfaces in the simulation.

With the tear added and the object distance assigned as 3 m, parameters of eye should be tweaked through an optimization based on the original eye model [18] focusing to the infinity, which is carried out under a constraint that the length of eye be 24 mm. Table 1 summarizes the optimized parameters, where AL and PL, in turn, denote the gradient refractive indices of anterior and posterior lenses. Besides, detailed parameters for aspherical surfaces and gradient lens are provided in Table 2 and Table 3, respectively.

Table 1. Parameters of optical surfaces used in Code V

Surface	Surface type	Radius (mm)	Thickness (mm)	Refractive index	Semi-aperture (mm)
object	sphere	infinity	3000		
1	asphere	7.7600	0.0130[b]	1.340	4.9510
2	asphere	7.7600	0.5500	1.376	4.9344
3	asphere	6.5200	3.0500	1.336	4.3777
4	Sphere	infinity	0	1.336	2.2928
5	asphere	14.3669	1.7136	AL	2.0569
6	sphere	infinity	1.3522	PL	0.0300[e]
7	asphere	-7.0081	17.3213	1.336	1.5423
8	sphere	-13.000	0.0000	1.336	12.5647

Table 2. Detailed parameters for aspherical surfaces

Surface	Y radius (mm)	Conic constant (K)	4th order coefficient	6th order coefficient
1	7.76	-0.1	0	0
2	7.76	-0.1	2.0e-5	0
3	6.52	-0.3	-2.0e-5	0
5	14.3669	-0.12	0.0012	-7.2440e-5
7	-7.0081	0.23	0.0005	4.3200e-5

Table 3. Coefficients of gradient refractive indices of lens

Coefficient	AL	PL
c_{10}	-0.1748e-02	
c_{20}	0.2180e-04	
n_{00}	1.376	1.416
c_{01}	0.04292	0
c_{02}	-0.01001	-0.4113e-02
c_{03}	-0.1292e-01	0
c_{04}	-0.707e-04	-0.3318e-03

Field of View: As illustrated in Fig. 5, FOV, whose vertex is situated at the center of entrance pupil, is the angle subtended by DOE. If measured diagonally, it could be determined by

$$FOV_D = 2\tan^{-1}\frac{\sqrt{W^2+H^2}}{2(d_{er}+d_{ep})} \tag{6}$$

where H is the vertical dimension of DOE, d_{er} the eye relief, and d_{ep} the distance from the vertex of tear to the center of entrance pupil, which is calculated as 3.05 mm. Say W=H= 38.4 mm and d_{er}= 12 mm, FOV is 122° (diagonal).

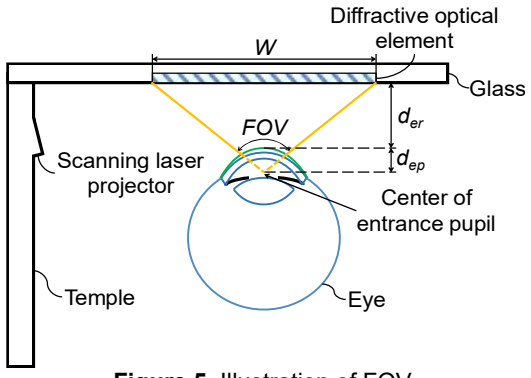

Figure 5. Illustration of FOV.

Angular Resolution: Angular resolution (AR) in arcminute (′) can be calculated as

$$AR = \frac{60 \cdot FOV}{N} = \frac{60 \cdot FOV}{\sqrt{N_h^2 + N_v^2}} \quad (7)$$

where N_h and N_v are the number of pixels along the horizontal and vertical directions, respectively. For FOV= 122°, N_h = 640, and N_v = 640, angular resolution 8.09′.

Diffraction Efficiency: In modeling the grating, wave optics module of COMSOL Multiphysics is used. The mode of wave is transverse electric. The diffraction order m is +1. The glass substrate of DOE is chosen as N-BK7 (Schott), whose refractive index is 1.5195 at 532 nm. Without loss of generality, 9 gratings are picked for simulation, as shown in Fig. 6. Say d_p= 10 mm, d_{doe}= 20 mm, and d_{lens}=16.73 mm, according to Eq. (4) and Eq. (5), the incident/diffraction angles θ_i/θ_m can be calculated. Based on the optimization, the optimal grating parameters and diffraction efficiencies (DEs) are obtained as in Table 4. The average DE, DE_{avg}, is 58.4%.

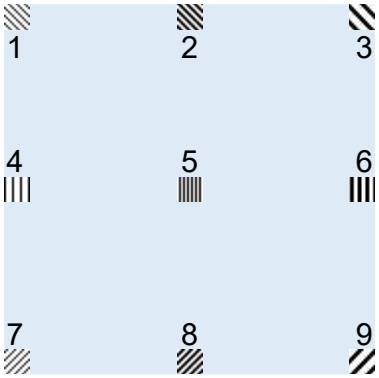

Figure 6. 9 gratings picked for simulation of FOV.

Table 4. Optimized parameters of gratings

#	θ_i (deg)	θ_1 (deg)	p (nm)	β (deg)	w_g (nm)	h_g (nm)	DE (%)
1	43.76	-34.34	423.6	50	157.4	500	58.71
2	59.93	-37.30	361.6	50	128.6	500	64.60
3	74.58	-55.55	297.4	37	117	500	60.22
4	63.44	48.93	3786.2	85	1327	500	58.33
5	75.69	0	549	62	218	500	52.35
6	80.28	-48.93	305.8	37	124.7	500	47.55
7	43.76	-34.34	423.6	50	157.4	500	58.71
8	59.93	-37.30	361.6	50	128.6	500	64.60
9	74.58	-55.55	297.4	37	117	500	60.22

Uniformity: As DE of each grating of DOE more or less differs, a figure of merit Γ to evaluate the uniformity is introduced as

$$\Gamma = 1 - \frac{\sigma}{DE_{avg}} \quad (8)$$

where σ is the standard deviation, formulated as

$$\sigma = \sqrt{\frac{1}{n}\sum_{i=1}^{n}\left(DE_i - DE_{avg}\right)^2} \quad (9)$$

where n is the number of gratings of interest, and i the serial number. Calculated with DEs in Table 4, the uniformity Γ is 0.91.

MTF: As shown in Fig. 7, modulation transfer functions (MTFs) are calculated as a function of spatial frequency in cycle/degree for the fields of 0° and 61° (tangential and radial). At 30 cycle/degree, which corresponds to the resolution limit of a normal eye, MTFs are above 0.9999 for all fields.

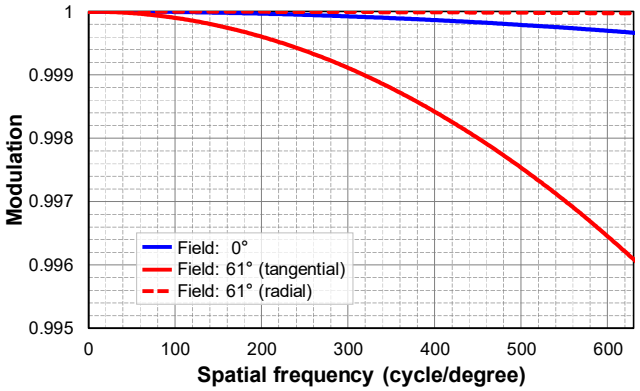

Figure 7. MTFs calculated for fields of 0° and 61°.

Contrast Ratio: Contrast ratio (CR) could be derived as

$$CR = \frac{CR_0 + 1 + (CR_0 - 1) \cdot MTF}{CR_0 + 1 - (CR_0 - 1) \cdot MTF} \quad (10)$$

where CR_o is the CR of scanning laser projector. For the field of 0°, CR_0= 5000, MTF= 0.9999, and CR is calculated as 4987, nearly the same as that of the projector.

Distortion: For the fact that the eye is far from being an ideal imaging system [22], distortion—the displacement of image height or ray location—is an inherent characteristic of all retinal projection based NEDs. As can be seen in Fig. 11, the distortion is 24%, give or take.

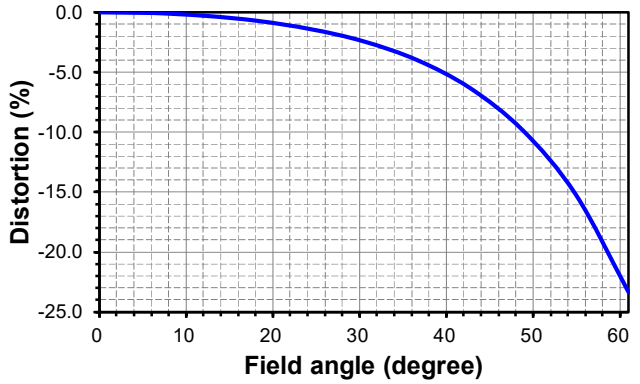

Figure 8. Distortion versus the field angle.

5. Conclusions

A lensless RSD, which is highlighted by a scanning laser projector, a DOE, and a wet eye, is proposed. To precisely model the eye, tear and gradient lens are taken into account. Based on the simulation, FOV is 122°, angular resolution is 8.09′, average DE of DOE is 58.4%, uniformity is 0.91, MTFs are above 0.9999 at 30 cycle/degree for all fields, distortion is 24%, and CR is 4987. Our RSD exhibits several unique features. First, no lens—except the lens of eye—is involved. The projected retinal image is focus free. Second, DOE is used as a combiner, making the device compact in design and suitable for see-through augmented reality. Third, the retinal image is immune to the change in the diopter of eye and pupil size.

6. Acknowledgments

National Natural Science Foundation of China (61831015); Science and Technology Commission of Shanghai Municipality (1801H163000, 1701H169200); Shanghai Rockers Inc. (15H100000157); Shanghai Jiao Tong University (AF0300204).

7. References

[1] L. Zhou, C. P. Chen, Y. Wu, K. Wang, and Z. Zhang, "See-through near-eye displays for visual impairment," in *23rd International Display Workshops in conjunction with Asia Display* (2016), pp. 1114–1115.

[2] L. Zhou, C. P. Chen, Y. Wu, Z. Zhang, K. Wang, B. Yu, and Y. Li, "See-through near-eye displays enabling vision correction," Opt. Express **25**(3), 2130–2142 (2017).

[3] A. Maimone, A. Georgiou, and J. S. Kollin, "Holographic near-eye displays for virtual and augmented reality," ACM Trans. Graph. **36**(4), 85 (2017).

[4] G.-Y. Lee, J.-Y. Hong, S. Hwang, S. Moon, H. Kang, S. Jeon, H. Kim, J.-H. Jeong, and B. Lee, "Metasurface eyepiece for augmented reality," Nat. Commun. **9**, 4562 (2018).

[5] T. Levola, "Diffractive optics for virtual reality displays," J. Soc. Inf. Disp. **14**(5), 467–475 (2006).

[6] H. Mukawa, K. Akutsu, I. Matsumura, S. Nakano, T. Yoshida, M. Kuwahara, and K. Aiki, "A full-color eyewear display using planar waveguides with reflection volume holograms," J. Soc. Inf. Disp. **17**(3), 185–193 (2009).

[7] Y. Wu, C. P. Chen, L. Zhou, Y. Li, B. Yu, and H. Jin, "Design of see-through near-eye display for presbyopia," Opt. Express **25**(8), 8937–8949 (2017).

[8] Y. Wu, C. P. Chen, L. Zhou, Y. Li, B. Yu, and H. Jin, "Near-eye display for vision correction with large FOV," in *SID Display Week* (2017), pp. 767–770.

[9] R. Sprague, A. Zhang, L. Hendricks, T. O'Brien, J. Ford, E. Tremblay, and T. Rutherford, "Novel HMD concepts from the DARPA SCENICC program," Proc. SPIE **8383**, 838302 (2012).

[10] A. Maimone, D. Lanman, K. Rathinavel, K. Keller, D. Luebke, and H. Fuchs, "Pinlight displays: wide field of view augmented reality eyeglasses using defocused point light sources," ACM Trans. Graph. **33**(4), 89 (2014).

[11] R. J. Jacobs, I. L. Bailey, and M. A. Bullimore, "Artificial pupils and Maxwellian view," Appl. Opt. **31**(19), 3668–3677 (1992).

[12] C. P. Chen, L. Zhou, J. Ge, Y. Wu, L. Mi, Y. Wu, B. Yu, and Y. Li, "Design of retinal projection displays enabling vision correction," Opt. Express **25**(23), 28223–28235 (2017).

[13] L. Mi, W. Zhang, C. P. Chen, Y. Zhou, Y. Li, B. Yu, and N. Maitlo, "A retinal-projection-based near-eye display for virtual reality," Proc. SPIE **10676**, 106761C (2018).

[14] Y. Wu, C. P. Chen, L. Mi, W. Zhang, J. Zhao, Y. Lu, W. Guo, B. Yu, Y. Li, and N. Maitlo, "Design of retinal-projection-based near-eye display with contact lens," Opt. Express **26**(9), 11553–11567 (2018).

[15] W. Zhang, Y. Wu, L. Mi, C. P. Chen, L. Zhong, B. Yu, Y. Li, and N. Maitlo, "Ultra-large field-of-view retinal projection display with vision correction," in *SID Display Week* (2018), pp. 1555–1558.

[16] W. Zhang, C. P. Chen, L. Mi, Y. Lu, M. Zhu, X. Ren, R. Tang, and N. Maitlo, "A retinal-projection-based near-eye display with contact lens for mixed reality," Proc. SPIE **11040**, 1104005 (2019).

[17] M. Farid, "The tear film: the neglected refractive interface," https://www.eyeworld.org/supplements/EW-September-supplement-2014.pdf.

[18] A. V. Goncharov and C. Dainty, "Wide-field schematic eye models with gradient-index lens," J. Opt. Soc. Am. A **24**(8), 2157–2174 (2007).

[19] Wikipedia, "Electron-beam lithography," https://en.wikipedia.org/wiki/Electron-beam_lithography.

[20] Z.-H. He, C.-P. Chen, J.-L. Zhu, Y.-C. Yuan, Y. Li, W. Hu, X. Li, H.-J. Li, J.-G. Lu, and Y.-K. Su, "Electrically tunable holographic polymer templated blue phase liquid crystal grating," *Chin. Phys. B* **24**(6), 064203 (2015).

[21] W. Zhou, *Nanoimprint Lithography: An Enabling Process for Nanofabrication* (Springer, 2013).

[22] M. Bass, C. DeCusatis, J. Enoch, V. Lakshminarayanan, G. Li, C. MacDonald, V. Mahajan, and E. V. Stryland, *Handbook of Optics 3rd Edition Volume III: Vision and Vision Optics* (McGraw-Hill Education, 2009).